

36. Peterson, A. M., Chen, K. S. & Linscott, I. R. in *IAU Symp.* 112, 373-384 (1985).
 37. Cullers, K. D. *IAU Symp.* 112, 385-390 (1985).
 38. Drake, F., Wolfe, J. H. & Seeger, C. L. (eds) *SETI Science Working Group Report* (NASA Tech. Pap. 2244, 1983).
 39. Seeger, C. L. & Wolfe, J. H. *IAU Symp.* 112, 391-398 (1985).
 40. Klein, M. J. & Gulkis, S. *IAU Symp.* 112, 397-404 (1985).
 41. Olsen, E. T., Lokshin, A. & Gulkis, S. *IAU Symp.* 112, 405-410 (1985).
 42. Gulkis, S. *IAU Symp.* 112, 411-418 (1985).
 43. Hart, M. H. *Q. Jl. R. astr. Soc.* 16, 128 (1975).
 44. Papagiannis, M. D. (ed.) *Strategies for the Search for Life in the Universe*, 13-76 (Reidel, Dordrecht, 1980).
 45. Hart, M. H. & Zuckerman, B. (eds) *Extraterrestrials, Where Are They?* (Pergamon, Oxford, 1982).
 46. Brim, G. D. *Q. Jl. R. astr. Soc.* 24, 283 (1983).
 47. Morrison, P. *IAU Symp.* 112, 13-20 (1985).
 48. Papagiannis, M. D. *IAU Symp.* 112, 505-512 and 543-546 (1985).
 49. Seeger, C. L. *IAU Symp.* 112, 487-492 (1985).
 50. Smith, H. J. *IAU Symp.* 112, 547-552 (1985).

ARTICLES

Intensive measurements of turbulence and shear in the equatorial undercurrent

M. C. Gregg*, H. Peters*, J. C. Wesson*, N. S. Oakey† & T. J. Shay*

* Applied Physics Laboratory and School of Oceanography, College of Ocean and Fishery Sciences, University of Washington, Seattle, Washington 98195, USA

† Bedford Institute of Oceanography, Dartmouth, Nova Scotia, Canada

Average profiles of turbulent dissipation rates provide tests of parameterizations used in numerical models. A strong diurnal mixing cycle is found in the well-stratified high-shear zone above the velocity maximum, and thermohaline intrusions are shown to be important mixing agents below the velocity maximum.

INTENSE and persistent mixing occurs in the equatorial undercurrents of the Atlantic and the Pacific oceans. Determining and parameterizing the average turbulent fluxes is necessary because these fluxes may provide the primary dynamical balance to the pressure gradient driving the undercurrent. Turbulent transport in the undercurrent is particularly important in the central Pacific, where it is a major factor controlling the tongue of cold water extending westward from South America¹. Temperature changes of the cold tongue affect the air-sea interactions that lead to anomalous weather conditions over North America. Therefore, improving the measurement and parameterization of the vertical turbulent fluxes in the undercurrent is a major goal of the Tropic Heat Program established to study the cold tongue¹. The undercurrent also provides an excellent natural laboratory for studying stratified turbulence.

Although the amount of previous turbulence data from the undercurrent is small, microstructure profiles taken at various locations and times, with different instruments, show similar patterns and intensities²⁻⁵. Earlier measurements with towed bodies report levels at the core of the undercurrent that are several decades higher than those observed with profilers^{6,7}, leading some to conclude that the towed data are badly contaminated by vibration and sensor difficulties^{2,5}. Others maintain that large intermittence at the velocity maximum produces the disparity⁸.

Between 25 and 30 November 1984, during the Tropic Heat field measurements, continuous profiling of turbulence was done in the upper 150 m at 0° N, 139°50' W with the advanced microstructure profiler (AMP)⁹. In 4.5 days, 385 drops were obtained, providing enough data to form accurate ensemble average profiles and to examine short-term fluctuations. Also, eight shear measurements were obtained with the expendable current profiler (XCP)¹⁰.

Background conditions

The average stratification and shear are typical of conditions near 0° N, 140° W. The mean stability frequency, \bar{N} , is low near the surface but increases rapidly, reaching a maximum of 0.02 s^{-1} near a pressure (p) of 1.0 MPa (corresponding to a depth of 100 m). Close to the surface the stratification is controlled by temperature, but salinity is important below 0.65 MPa. Because the XCP measures relative velocities, the average speed between 5.0 and 5.5 MPa is set to zero, in general agreement with mooring observations. Useful signals from the XCP begin at 0.3 MPa;

the transport at shallower depths is to the west, as observed from the ship drift. The zonal flow below 0.3 MPa is eastward (zonal velocity $\bar{U} > 0$ in Fig. 1), reaching 1.6 m s^{-1} near 1.05 MPa, which is close to the depth of the salinity maximum. Owing to the proximity of the magnetic equator the north component of the XCP signal is not useful. Nevertheless, because of the dominance of the eastward flow, good estimates of shear are obtained from $\partial \bar{U} / \partial z$ (where z is the depth). Values are calculated from the slopes of linear fits to the raw velocity components. The interval of each fit is 0.2 MPa, and a fit is done every 0.05 MPa. Shear decreases with depth and has a local minimum at the velocity maximum. Because this occurs close to N_{max} , the Richardson number, $Ri = \bar{N}^2 (\partial \bar{U} / \partial z)^{-2}$, has a sharp maximum. Above 0.5 MPa, $Ri < 0.25$; between 0.5 and 0.9 MPa, it is about 0.35 (Fig. 2). Based on fluctuations in the eight shear profiles used to form the average, we estimate typical confidence limits to be (0.0-0.15) for $Ri = 0.07$ and (0.2-0.5) for $Ri = 0.3$. Vertical smearing, due to displacements by internal waves and the internal tide, makes the velocity maximum appear thicker and reduces the maximum value. $Ri < Ri_{\text{cr}} = 0.25$ is a necessary but not sufficient condition for instability of laminar flows¹¹.

Average mixing rates above velocity maximum

Centimetre-scale gradients of horizontal velocity and temperature measured with AMP are used to compute the variances of the gradients over successive 0.005 MPa (0.5-m) sections. Scaling yields $\epsilon = 7.5\nu \langle (\partial U' / \partial z)^2 \rangle$ and $\chi = 6\kappa_T \langle (\partial T' / \partial z)^2 \rangle$. ϵ is the rate of viscous dissipation of turbulent kinetic energy, and χ is the rate of diffusive smoothing of turbulent temperature fluctuations. (ν is the kinematic viscosity and κ_T is the thermal diffusivity.) In both cases, isotropy of the microscale gradients is assumed.

Because of the large number of records taken in a short time, average profiles of ϵ and χ can be formed using all data in each 0.005 MPa pressure bin (Fig. 3). Comparison with laboratory results provides a measure of the relative intensity of $\bar{\epsilon}$. Studies of decaying grid turbulence in unsheared flows¹² show that when $\epsilon > \epsilon_{\text{cr}} = 24.5\nu N^2$, the turbulence will be sufficiently intense to produce a negative buoyancy flux, that is, $J_b = -g\rho^{-1}w'\rho' < 0$ where g is the gravitational acceleration, ρ' is the density and w' is the vertical velocity. A negative buoyancy flux corresponds to an upward mass flux, which increases the mean potential energy. Preliminary results from sheared flows¹³ show that the

Fig. 1 Average profiles of the stratification and velocity fields; θ is potential temperature, s is salinity (in concentration units), σ_θ is potential density, p is pressure, and U is the zonal velocity (positive east). These plots are formed from averages of 385 AMP profiles and eight XCP profiles. Owing to vertical displacement by internal waves and the internal tide, averaging smooths small-scale structures in these profiles. Both the depth of the velocity maximum, 1.1 MPa (110 m), and its association with the salinity maximum are typical near 0° N, 140° W. The stability frequency, N , is computed from the average temperature and salinity profiles and peaks slightly above the velocity maximum, producing a sharp maximum in the Richardson number, Ri .

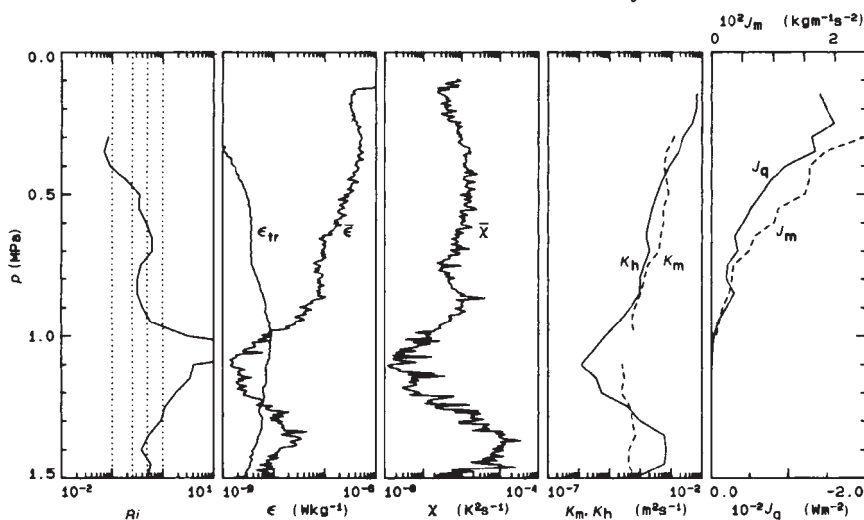
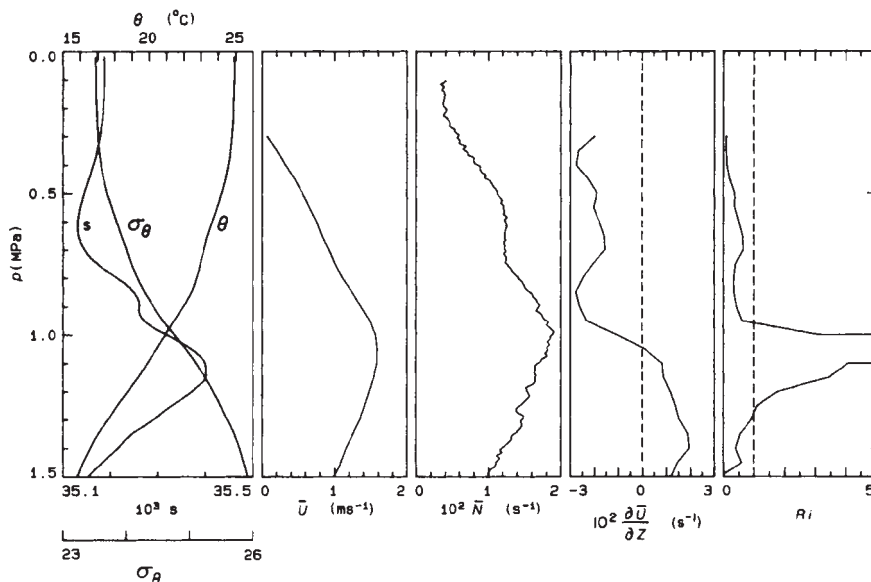


Fig. 2 The average Richardson number, Ri , and dissipation rates. Where $Ri < 1$, $\bar{\epsilon}(p) > \epsilon_{tr}$, the threshold for active turbulence. $\bar{\chi}(p)$ follows a similar pattern, modified by the local temperature gradient. The turbulent eddy coefficients for heat, K_h , and momentum, K_m (dashed line), are approximately equal between 0.3 and 0.9 MPa. The corresponding turbulent fluxes, J_q and J_m (dashed line), follow similar patterns, having large values near 0.3 MPa and decaying to about 0 at the Ri maximum.

same criterion holds when $Ri > 0.25$; when $Ri < 0.25$ the turbulence does not decay.

In the undercurrent, $\bar{\epsilon}$ decreases with depth (Fig. 2). Above 0.4 MPa, $Ri < 0.1$ and $\bar{\epsilon}$ exceeds ϵ_{tr} by at least two decades. This ratio decreases to about 20 between 0.6 and 0.9 MPa, where $1/4 < Ri < 1/2$. It then drops rapidly and crosses 1 where $Ri = 1$. Thus, in most of the high-shear zone above the velocity maximum the average dissipation rates indicate strongly active turbulence, producing a net buoyancy flux.

In steady, homogeneous turbulence, the balance equation for turbulent kinetic energy reduces to local production and dissipation. If the mean shear is strong, the turbulent production can be expressed as a vertical eddy coefficient for momentum, K_m

$$K_m = \frac{\epsilon}{(1 - R_f) (\partial \bar{U} / \partial z)^2} \text{ m}^2 \text{ s}^{-1} \quad (1)$$

where R_f is the flux Richardson number. Because $R_f \leq 0.15$ this term is a small correction and is ignored. The corresponding vertical momentum flux is

$$J_m = -\rho K_m \frac{\partial \bar{U}}{\partial z} \text{ kg m}^{-1} \text{ s}^{-2} \quad (2)$$

In studies of the planetary boundary layer of the atmosphere, this procedure is known as the dissipation method and has been verified by comparison with direct flux measurements. If the temperature fluctuations are produced by turbulent overturns against the mean gradient, rather than by lateral advection, a similar balance applies with the \bar{T}^2 -balance equation, yielding

the turbulent transport coefficient for heat, K_h , and the vertical turbulent heat flux, J_q :

$$K_h = \frac{\chi}{2(\partial \bar{T} / \partial z)^2} \text{ m}^2 \text{ s}^{-1} \quad (3)$$

$$J_q = -\rho C_p K_h \frac{\partial \bar{T}}{\partial z} \text{ W kg}^{-1} \quad (4)$$

This approach, known as the Osborn-Cox method¹⁴, is widely used to obtain turbulent heat fluxes in the thermocline.

Equations (1) and (3) have been used with previous measurements in the undercurrent to develop parameterizations for numerical models^{15,16}. Their use has not been verified in the ocean by comparison with direct flux measurements, but conditions between 0.3 and 0.9 MPa are more appropriate to the dissipation method than any other known section in the ocean, and the present data offer much greater statistical confidence than previously available. Above 0.9 MPa, K_m and K_h are nearly equal, that is, the turbulent Prandtl number is close to one, and they decrease rapidly with depth. At 0.3 MPa, $K_m \approx K_h \approx 2 \times 10^{-3} \text{ m}^2 \text{ s}^{-1}$, and at 0.9 MPa, $K_m \approx K_h \approx 6 \times 10^{-5} \text{ m}^2 \text{ s}^{-1}$, a decrease by a factor of 25. Over the same interval, J_q drops from 140 to 20 W m^{-2} . (J_q decreases relatively less than K_h because $\partial \bar{T} / \partial z$ also decreases.)

Average mixing rates at velocity maximum

At the velocity maximum, the dissipation rate has a minimum, $\bar{\epsilon} = 2 \times 10^{-9} \text{ W kg}^{-1}$, which is about a quarter of ϵ_{tr} . Because $\epsilon < \epsilon_{tr}$, dissipation-scale fluctuations are less likely to be isotropic

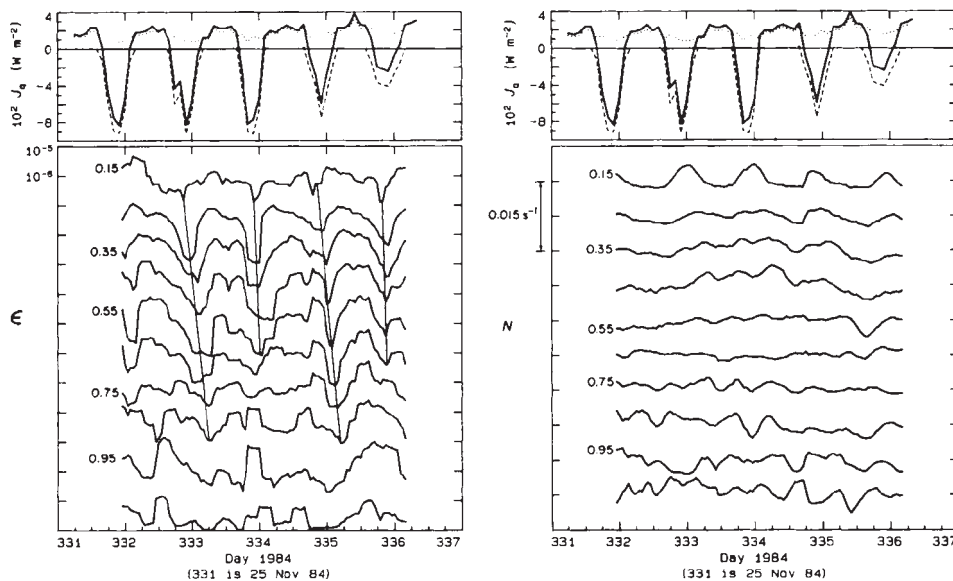


Fig. 3 Five-hour running means of the surface heat flux, of ϵ , and of N , showing a diurnal cycle in ϵ penetrating deep into the thermocline. The surface heat flux (solid line in the top panels) is dominated by the short-wave radiation (dashed), and by the latent heat flux (dotted). The time series for ϵ and N are averages over successive 0.1-MPa intervals; for example, the first set, labelled 0.15, are averages between 0.1 and 0.2 MPa. The curves for pressures >0.15 MPa are successively offset by one decade in ϵ and N , respectively. The diurnal cycle in ϵ remains distinct to 0.65 MPa and has some deeper signatures, unlike the diurnal N cycle, which is weak at 0.25 MPa and absent deeper. The daily minimum in ϵ has a progressive phase lag with depth, as shown by the slanting lines.

than at shallower depths. The maximum effect of anisotropy is to reduce $\bar{\chi}$ by a factor of 3. The effect on $\bar{\epsilon}$ is more difficult to estimate, but should be at least as large. Thus, if the microstructure at the core is anisotropic in the dissipation range, $\bar{\epsilon}$ and $\bar{\chi}$ will be even smaller compared with the levels in the high-shear zone shown in Fig. 2.

To remove the effects of displacements by internal waves and the internal tide, a preliminary statistical analysis was done on all 0.5-m ϵ values between potential density, $\sigma_\theta = 24.6$ and 25.5, which spans the velocity maximum. This yields $\bar{\epsilon} = 4.7 \times 10^{-9} \text{ W kg}^{-1}$ which is only a factor of three higher than an average found in a quiet region of the California Current¹⁷ and is almost three decades lower than the values reported from towed measurements^{6,7}. A probability distribution does not reveal any greater degree of intermittence than in other locations. For example, using the standard deviation of $\ln \epsilon$ as the measure of intermittence⁸, $\sigma_{\ln \epsilon} = 2.4$ compared with $\sigma_{\ln \epsilon} = 2.3$ from the California Current¹⁷. Using this in the maximum-likelihood estimate suggested for intermittent turbulence⁸ yields a value smaller than the arithmetic mean, that is, $\epsilon_{\text{mle}} = 4.2 \times 10^{-9} \text{ W kg}^{-1}$, because the distribution is skewed to low values and has a median of $2.2 \times 10^{-10} \text{ W kg}^{-1}$. Therefore, these data do not reveal unusual intermittence at the velocity maximum, but indicate that the conditions are similar to those in the main thermocline at less energetic locations.

Because the shear passes through zero, conditions are not appropriate for the dissipation method, and K_m is not calculated. The estimate of K_h is not affected, however, because the temperature gradient remains large, and $K_h \approx 1 \times 10^{-6} \text{ m}^2 \text{ s}^{-1}$. This is about 10 times κ_T , the molecular diffusion coefficient, and provides additional evidence that mixing levels at the velocity maximum are weak.

The diurnal cycle

Daily fluctuations, by factors of 10 to 100 in ϵ and χ , exist both in the diurnal mixed layer and in the well-stratified profile below (Fig. 3). The cycle extends to between 0.75 and 0.95 MPa, even though day-to-day variability not related to changes in the surface heat flux is also apparent.

Between 0.1 and 0.3 MPa, both the mixing and the stratification change in phase with the surface heat flux, which is dominated by the short-wave radiation and the latent heat flux. (The sensible heat flux is negligible by comparison, varying between -12 and $+20 \text{ W m}^{-2}$.) At night, the net flux is $\approx 200 \text{ W m}^{-2}$ out of the sea, corresponding to a surface buoyancy flux of $J_b^0 = 3.2 \times 10^{-7} \text{ W kg}^{-1}$, producing a well-mixed layer extending to between 0.2 and 0.3 MPa.

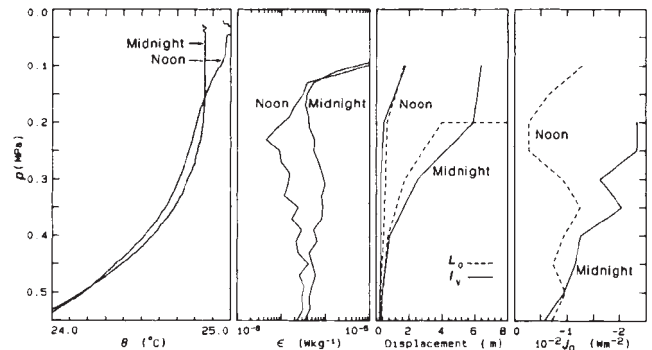
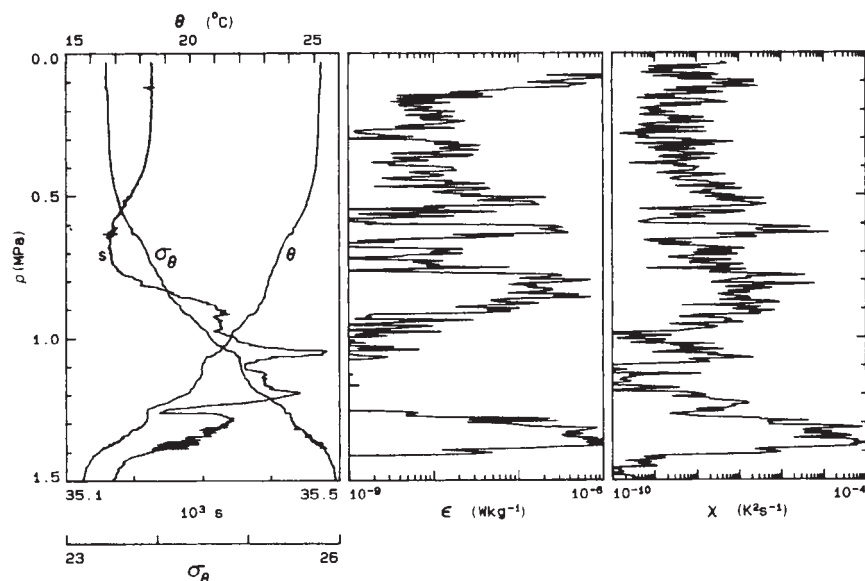


Fig. 4 Comparison of the averages of all profiles within 1 h of local noon and of local midnight. The mixed layer extends to 0.2 MPa at midnight, but is fully restratified by noon. Above 0.1 MPa the mixing rates are dominated by wind forcing, but between 0.15 and 0.65 MPa the diurnal cycle is evident. At noon, the turbulence is most heavily suppressed near 0.25 MPa. The observed vertical displacements, l_v , are independent measures of changes in ϵ and agree well with the Ozmidov scale, L_0 , computed from the dissipation rates and stratification. At 0.25 MPa, the turbulent heat flux, J_q , drops from 240 W m^{-2} at midnight to 30 W m^{-2} at noon.

Observations in another convecting mixed layer show $\bar{\epsilon} \approx J_b^0$ within the mixed layer and below the zone affected by the wind¹⁸. In this case, which was in a region with a moderate mean shear, the dissipation layer terminated in a sharp density step and the dissipation rates below the entrainment zone decreased several decades. A profile of $\bar{\epsilon}$ for midnight shows a minimum of $4 \times 10^{-7} \text{ W kg}^{-1}$ below the surface zone, followed by an increase to $1 \times 10^{-6} \text{ W kg}^{-1}$ at 0.3 MPa (Fig. 4). Thus, the turbulence produced by convection may account for a substantial fraction of the observed $\bar{\epsilon}$ above 0.3 MPa, but production by the mean shear or wind mixing is also present. The shape of the average midnight temperature profile is similar to individual realizations and shows a smooth transition to the stratified regime. This is very different from the abrupt termination of convecting mixed layers where the deeper water has low dissipation rates¹⁸. We believe this is due to the intense turbulence in the stratified section as well as in the mixed layer. Above 0.3 MPa, $\bar{\epsilon}$ is a minimum at noon, when the profile has maximum stratification.

Below 0.3 MPa the diurnal $\bar{\epsilon}$ cycle remains large and is 1.5 decades at 0.65 MPa (Fig. 3), even though there is day-to-day

Fig. 5 An AMP drop showing multiple salinity maxima and minima below 1 MPa, indicating the importance of lateral advection. The deepest of the three intrusions occurs where $Ri < 1$ and has strong mixing between 1.25 and 1.4 MPa, where the profile is diffusively unstable to salt fingering. The pattern of activity is similar to that found in highly sheared intrusions in a warm-core Gulf Stream ring¹⁶. This profile was taken at 20.53 GMT, or 10.53 LT, and has relatively weak dissipation rates between 0.3 and 0.9 MPa and on the intrusions where $Ri > 1$.



variability. The cycle is not symmetric, but has maxima lasting longer than the minima. Examination of more detailed plots shows that decreases in ϵ begin nearly simultaneously with depth. Nevertheless, the minimum has a phase lag that increases downward (Fig. 3). At 0.65 MPa, the lag is 3–6 h after local noon.

Between 0.3 and 0.9 MPa the diurnal cycles in ϵ and χ produce large changes in the overturning scales of the turbulence and in J_q (Fig. 4). Two measures of overturning are used: the Ozmidov scale, $L_o = \epsilon^{1/2} N^{-3/2}$, and l_n , the root-mean-square displacement computed by comparing the observed σ_θ profiles with resorted monotonic versions of the same data^{19,20}. The two scales show good agreement. Below 0.3 MPa, the overturning scales at noon are only a few tens of centimetres, but, during the night, they grow to a few metres. Correspondingly, J_q increases from about 30 W m^{-2} at noon to about 240 W m^{-2} at midnight. At night these estimates are unreliable above 0.25 MPa owing to the weak stratification in the mixed layer.

Thermohaline intrusions from 1.0 to 1.5 MPa

Between 1.0 and 1.5 MPa, thermohaline intrusions strongly affect ϵ and χ . Although temperature usually decreases monotonically over scales greater than 1 m, salinity has a sequence of maxima and minima (Fig. 5). These can only be of advective origin, and are probably associated with the salinity front near the Equator²¹. Changes between successive profiles indicate that the intrusions have horizontal scales less than a few kilometres. Very high dissipation rates occur beneath the salinity maximum of some intrusions. For example, comparing Fig. 5 with the average profiles in Fig. 2 shows that between 1.3 and 1.4 MPa ϵ is as high as $\bar{\epsilon}$ at 0.3 MPa, and χ is higher than $\bar{\chi}$. A similar pattern, found on thermohaline intrusions in a warm-core ring, was attributed to a combination of salt fingering and the shear of near-inertial motions²². Because strong lateral processes, and possibly salt fingering, are involved, neither the dissipation method nor the Osborn–Cox model are applicable to the mean profiles in this pressure range.

Discussion

Based on profiles of $\bar{\epsilon}$ and $\bar{\chi}$, five mixing zones are found in the upper 1.5 MPa below the near-surface zone: (1) the diurnal mixed layer, 0.1–0.3 MPa, has high dissipation rates, which are modulated by almost a factor of 100 and are in phase with the surface heat flux; (2) the upper high-shear zone, 0.3–0.9 MPa, has dissipation rates and turbulent fluxes that are high just below the mixed layer but decrease with depth, as Ri increases. At a given depth, the dissipation rates vary by factors of 10 to 100

in a diurnal cycle; (3) the velocity maximum, 0.9 to 1.25 MPa, has low dissipation rates, similar to those in mid-gyre; and (4) the lower high-shear zone, 1.25 to 1.5 MPa, has high dissipation rates when thermohaline intrusions occur.

The patterns and magnitudes of these observations are consistent with previous profiles in the undercurrent and are inconsistent with the towed observations. Discovery of the diurnal cycle in the stratified region below the surface mixed layer and of the role of thermohaline intrusions in the dissipation below the core is new.

The daily ϵ cycle is nearly as strong between 0.3 and 0.65 MPa as in the diurnal mixed layer. This is a surprise in view of the restricted depth range of the diurnal cycle in stratification. N variations are readily apparent (Fig. 3), but they have no diurnal signature similar to that in ϵ and χ . To our knowledge no previous observations have been reported, from any location, of a diurnal cycle below the mixed layer and its entrainment zone.

We have considered several possible causes of the deep diurnal mixing cycle: the absorption of solar radiation, a diurnal cycle in the large-scale shear, and daily modulation of high-frequency internal waves.

Suppression of the turbulence by a buoyancy flux resulting from the absorption of solar radiation seemed a likely mechanism when we noticed the diurnal cycle at sea and has since been suggested to us by several others (M. Lewis and J. D. Woods, personal communications). We do not, however, understand how this can happen without also producing a daily cycle in N , which is not apparent in Fig. 3 or in other more detailed plots.

No diurnal shear cycle has been reported from the Equator; but, in response to discovery of the diurnal mixing cycle, current meter records from moorings at 0° N , 140° W in May and November 1983 have been examined (D. Halpern, personal communication). Between 0.1 and 0.25 MPa, shear has a strong daily fluctuation, $\sim 0.01 \text{ s}^{-1}$, but this decreases rapidly with depth and is negligible below the diurnal mixed layer, especially compared with the semi-diurnal tidal signal.

Internal wave energy on the equator is higher than found in mid-gyre²³, and laboratory studies show that mixed layer turbulence can generate internal waves in the thermocline²⁴. Therefore, internal waves, generated when turbulence is strong in the mixed layer, may propagate downward and break in the stratified high-shear zone, producing much of the observed mixing. When the surface layer restratifies during the day the source of internal waves will be suppressed, leading to a minimum in mixing below the mixed layer which may have a phase lag as the effect propagates downward.

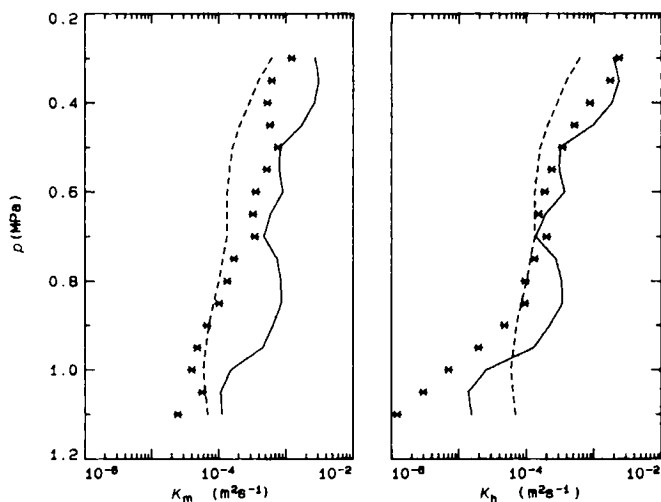


Fig. 6 Comparison of K_m and K_h obtained using the dissipation method (*) with parameterizations used in two numerical models of the undercurrent. Dashed line, from ref. 15; solid line, from ref. 16. The model K_m and K_h are functions of the observed $\bar{N}(p)$ and/or $Ri(p)$. The parameterizations are closer where Ri is low, above 0.7 MPa, than where Ri is high.

The data available to us are inadequate to determine whether one of these mechanisms is the cause, because small changes in either N or shear could be responsible. Mixing in this zone resembles a sharply tuned harmonic oscillator, which can have large output changes for small forcing perturbations. Plotting the $\bar{\epsilon}$ profile as a function of Ri shows a large increase when Ri drops below 0.25. Consequently, a 20% increase in shear or a similar decrease in N can change the average Richardson number from 0.35 to 0.25. Figure 3 shows much larger changes occurring in N , but with no apparent daily frequency. The eight XCP profiles show that the shear also changes by more than 20%. Because a wide band of frequencies seem to contribute to changes in both N and shear, longer time series of both are needed to define a diurnal signature. Data taken by other Tropic Heat investigators may be able to resolve this, but we know of no measurements that can examine the role of high-frequency internal waves and recommend that such measurements be included in future experiments.

In addition to taking the time series on the Equator we made measurements at 0.5° intervals off the Equator and found that the diurnal cycle extended to at least 1.0 MPa just outside of the undercurrent, compared with 0.3 MPa, in the centre of the undercurrent. It is possible that internal waves radiated from these deeper layers are also involved and that the problem is three-dimensional rather than just one-dimensional.

Received 5 June; accepted 28 August 1985.

- Eriksen, C. C. *EOS* **66**, 50-51 (1985).
- Gregg, M. C. *J. geophys. Res.* **81**, 1180-1196 (1976).
- Crawford, W. R. & Osborn, T. R. *Deep-Sea Res.* GATE suppl. 2 to vol. **26**, 285-308 (1979).
- Crawford, W. R. *J. phys. Oceanogr.* **12**, 1137-1149 (1982).
- Paka, V. T., Vasilenko, V. M., Osadchiy, A. S. & Shkurenko, V. I. in *Variability of the Ocean and Atmosphere in the Equatorial Atlantic* (ed Monin, A. S.) 78-105 (Nauka, Moscow, 1982).
- Belyayev, V. S., Lyubimov, M. M. & Ozmidov, R. V. *Izv. Atmos. Ocean. Phys.* **9**, 1179-1185 (1973).
- Williams, R. B. & Gibson, C. H. *J. phys. Oceanogr.* **4**, 104-108 (1974).
- Gibson, C. H. in *Hydrodynamics of the Equatorial Ocean* (ed Nihoul, J. C. J.) 131-153 (Elsevier, Amsterdam, 1983).
- Gregg, M. C., Nodland, W. E., Aagaard, E. E. & Hirt, D. H. *Oceans '82 Conf. Rec. IEEE* Cat. No. 82CH1827-5, 260-265 (Marine Technology Society, Washington DC 1982).

Two recent numerical models of the undercurrent are based on previous microstructure observations. One parameterizes the eddy coefficients in terms of N , largely for mathematical convenience¹⁵

$$K_m = K_h = AN^{-2} \quad (5)$$

with A chosen to produce $K_m = 5.5 \times 10^{-5} \text{ m}^2 \text{ s}^{-1}$ at N_{max} . Another¹⁶ bases the parameterization on Ri

$$K_m = 1 \times 10^{-4} + \frac{5.5 \times 10^{-3}}{(1 + 5 Ri)^2} \quad (6)$$

and

$$K_h = 1 \times 10^{-5} + \frac{K_m}{1 + 5 Ri} \quad (7)$$

Comparison with our estimates, using equations (1) and (3), shows that equation (6) is consistently high, except between 0.5 and 0.7 MPa (Fig. 6). Equation (7) agrees remarkably well with observations above 0.7 MPa, but is an overestimate at greater depths. Equation (5) agrees relatively well with observations for K_m , but is low by factors of 2-5 between 0.4 and 0.7 MPa. For K_h , equation (5) has much less vertical change than the observations, and crosses from an under to an over estimate near 0.7 MPa. At 1.1 MPa, it is almost a factor of 100 too high.

Both parameterizations are in rough agreement with K_m and K_h computed from our data and equations (1) and (3), but neither is a good fit. The major discrepancies are overestimation of both eddy coefficients at the velocity maximum (the additive terms are much too large) and underestimation of the increases in K_m and K_h when Ri drops below 0.25. A plot of K_m and K_h as functions of Ri shows that they rise abruptly by about a factor of 10 when Ri approaches 0.25. Because a large section of the mixing region is in this Richardson number range, improving this part of the parameterization is particularly important.

Until the diurnal cycle is understood, these parameterizations, which are based on only the large-scale profiles, must be viewed as tentative. If fluctuating internal wave energy or the absorption of solar energy has a major role, a simple Ri parameterization will be inadequate. Discovery of the diurnal cycle also raises the possibility of an annual cycle, because the intensity of the diurnal cycle may vary with season.

We thank Captain Clampitt and the officers and crew of the RV *Thomas G. Thompson* for their cooperation at sea and Wayne Nodland, Dale Hirt, Earl Krause, Matt Nicholas, Pat McKeown, Steve Sova and Thomas Bongers for careful work in collecting the data, and also David Halpern for examining his previous equatorial shear data. This work was funded by the NSF on grant OCE-8214780, as part of the Tropic Heat Program. School of Oceanography, University of Washington, contribution no. 1597.

- Sanford, T. B., Drever, R. G., Dunlap, J. H. & D'Asaro, E. A. *Design, Operation and Performance of an Expendable Temperature and Velocity Profiler*, APL-UW 8110 (Applied Physics Laboratory, University of Washington, Seattle, 1982).
- Howard, L. N. *J. Fluid Mech.* **10**, 509-512 (1961).
- Stillinger, D. C., Helland, K. N. & Van Atta, C. W. *J. Fluid Mech.* **131**, 91-122 (1983).
- Rohr, J. J., Helland, K. N., Itsweire, E. C. & Van Atta, C. W. *5th Symp. on Turbulent Shear Flows*, Cornell (submitted).
- Osborn, T. R. & Cox, C. S. *Geophys. Fluid Dyn.* **3**, 321-345 (1972).
- McCreary, J. P. *Phil. Trans. R. Soc.* **A298**, 603-635 (1981).
- Pacanowski, R. C. & Philander, S. G. H. *J. phys. Oceanogr.* **11**, 1443-1451 (1981).
- Gregg, M. C., D'Asaro, E. A., Shay, T. J. & Larson, N. J. *J. phys. Oceanogr.* (submitted).
- Shay, T. J. & Gregg, M. C. *Nature* **310**, 282-285 (1984).
- Thorpe, S. A. *Phil. Trans. R. Soc.* **286**, 125-181 (1977).
- Dillon, T. M. *J. geophys. Res.* **87**, 9601-9613 (1982).
- McPhaden, M. J. *J. geophys. Res.* (in the press).
- Larson, N. G. & Gregg, M. C. *Nature* **306**, 26-32 (1983).
- Hayes, S. P. & Powell, C. J. *J. geophys. Res.* **85**, 4029-4035 (1980).
- Linden, P. F. *J. Fluid Mech.* **71**, 385-405 (1975).